

Published in final edited form as:

J Magn Reson Imaging. 2014 October ; 40(4): 832–838. doi:10.1002/jmri.24441.

Quantification of Amide Proton Transfer Effect Pre- and Post-Gadolinium Contrast Agent Administration

Y.K. Tee^{1,2,*}, Manus J Donahue³, George Harston⁴, S. J. Payne¹, and M. A. Chappell¹

¹Institute of Biomedical Engineering, Department of Engineering Science, University of Oxford, UK

²Centre for Doctoral Training in Healthcare Innovation, University of Oxford, UK

³School of Medicine, Vanderbilt University, Nashville, Tennessee, US

⁴Acute Stroke Programme, Radcliffe Department of Medicine, UK

Abstract

Purpose—To compare quantification of the amide proton transfer (APT) effect pre- and post-gadolinium contrast agent (Gd) administration, in order to establish to what extent Gd alters quantification of the APT effect.

Materials and Methods—Four patients with internal carotid stenosis were recruited. APT imaging was acquired pre- and post-contrast in two sessions (before and after surgery) to assess the extent of relaxation time, T_1 , change on APT effect calculated using magnetization transfer ratio asymmetry analysis at offsets of ± 3.5 ppm relative to water resonance. Statistical and modelling evaluations were performed on the pre- and post-contrast APT effect to study the sensitivity to contrast administration.

Results—Before surgery, the post-contrast T_1 was estimated to drop $<10\%$ of the pre-value for the majority of the patients. After surgery, higher post-contrast T_1 reductions were observed in all the patients (maximum decrease was about 20% of the pre-value). Consistent differences between pre- and post-contrast were seen in the APT effect quantified using the asymmetry measure in most regions of the brain, with significant differences found in the white matter at the group level and in 25% of the individual patient results.

Conclusion—APT imaging should be performed prior to Gd administration to avoid potential misinterpretation of the APT effect.

Keywords

Amide proton transfer (APT) imaging; chemical exchange saturation transfer (CEST) imaging; magnetization transfer (MT) imaging; gadolinium contrast agents

*Correspondence to: Yee Kai Tee, Institute of Biomedical Engineering, Department of Engineering Science, Old Road Campus Research Building, University of Oxford, Oxford OX3 7DQ, UK. Phone: +441865617660, Fax: +441865617701, teeyekai@gmail.com.

Introduction

Gadolinium contrast agents (Gd) are widely used in clinical MRI to increase the contrast for angiography and tumour diagnosis, and to improve cerebral perfusion assessment. It is widely known that the administration of Gd will reduce the longitudinal relaxation time of water protons, T_1 (1,2). A study of T_1 pre- and post-Gd administration on blood showed that the reduction could be more than 50% of the pre-contrast value at 3T even 30 minutes after infusion (1).

Amide proton transfer (APT) imaging is an emerging chemical exchange saturation transfer (CEST) MRI technique for pH mapping that has potential clinical applications in penumbra identification following ischemic stroke (3–6), in discrimination of tumour and radiation necrosis (7) or normal tissue (8), and tumour grading in brain tumour patients (9,10).

The magnetization transfer ratio asymmetry analysis (MTR_{asym}) is T_1 dependent (3), hence may be affected by the presence of residual Gd in post-contrast imaging. However, to date no study has compared the differences in APT imaging before and after Gd administration to determine whether the effect is significant or the sensitivity to contrast is of concern in clinical protocols since perfusion weighted imaging using Gd is often acquired in stroke assessment and Gd enhanced T_1 -weighted imaging improves cancer diagnosis when used in conjunction with other conventional MRI techniques. This information is particularly pertinent to compare the efficacy of APT and Gd-based imaging since post-contrast APT imaging may be affected by the presence of residual Gd.

In this study, APT data were acquired in patients with internal carotid stenosis pre- and post-contrast to examine the extent of T_1 change on MTR_{asym} and to determine whether APT imaging should be performed pre-contrast to avoid potential misinterpretation of the APT effect.

Materials and Methods

Simulation

The Bloch-McConnell equations were used to simulate the effect of T_1 changes on the z -spectrum. A three-pool model consisting of water protons (w), amide protons ($labile$) and magnetization transfer (MT) plus nuclear overhauser effects (MT+NOE) following (11) was used to generate the z -spectra in MATLAB (Mathworks, Natick, MA, USA). A pulsed saturation scheme was simulated at 3T with 50 Gaussian pulses, where each pulse had a flip angle of 184° and pulse cycle of 40 ms with 50% duty cycle. The pulses were discretized into 1024 segments and crusher gradients with alternating signs applied during the inter-pulse delays were modeled by setting the transverse magnetization to zero (12). The saturation was applied from -4.5 to 4.5 ppm with 0.3 ppm increments. It was assumed that the readout was performed after all the pulses had been applied to match the 2D APT sequence used in the experimental data.

The water proton relaxation time, T_{1w} was set to 1.3 s (13) for the pre-contrast value and different post-contrast times were simulated varying from 10 to 50 % less than the pre-value.

Root mean square (RMS) differences between the pre- and different post-contrast z-spectra were calculated to form a linear relationship between the percentage reduction in the T_1 of water and the effect on the spectrum. The rest of the parameters in the model were assumed to be unaffected by the introduction of Gd and set according to the literature (11,14,15): longitudinal relaxation times, $T_{1labile} = 0.77$ s, $T_{1(MT+NOE)} = 1$ s; transverse relaxation times, $T_{2w} = 50$ ms, $T_{2labile} = 10$ ms, $T_{2(MT+NOE)} = 0.2$ ms; proton exchange rate, $k_{labile} = 28$ s⁻¹, $k_{(MT+NOE)} = 40$ s⁻¹; proton concentration, $M_{w0} = 111.2$ M, $M_{labile0} = 72$ mM, $M_{(MT+NOE)0} = 7.15$ M; chemical shifts, $\omega_w = 0$ ppm, $\omega_{labile} = 3.5$ ppm, $\omega_{(MT+NOE)} = -2.41$ ppm.

MRI Experiment

Four patients who were to undergo carotid endarterectomy provided informed consent and were scanned at 3T (Siemens Verio) using APT and diffusion-weighted imaging (DWI) sequences, according to a research protocol approved by the Institutional Review Board, both before and after surgery. A T_1 structural image with pixel dimensions = 1.72 x 1.72 x 2 mm was also acquired in each patient. The DWI data were acquired before the contrast infusion using b values of 0 and 1000, matrix size = 128 x 128 x 27 and spatial dimensions = 1.5625 x 1.5625 x 4.5 mm³.

APT data were collected pre and post intra-venous bolus injection of 0.1 mmol/kg 0.5M chelated Gd followed by a 20 ml saline flush. The post-contrast scan was acquired approximately 3 minutes after Gd administration given during a dynamic susceptibility contrast scan (DSC), as would be typical in a clinical scenario. Single slice transverse imaging was performed mid brain for the APT data with TR/TE=4000/26 ms, matrix size = 80 x 80 and pixel dimensions = 3 x 3 x 5 mm. The APT saturation was performed using the following RF parameters: 50 Gaussian pulses with flip angle = 184° and duration of 20 ms with 20 ms spacing each, to achieve an equivalent continuous saturation B_1 value of 0.535 μ T (average power). Data were acquired for saturation frequency offsets from -4.5 to 4.5 ppm with 0.3 ppm increment plus a unsaturated image, resulting in 32 volumes acquired in 2 min 55 s.

Data Processing and Analysis

Motion artefacts were corrected using FMRIB's Linear Image Registration Tool (FLIRT) in the FSL package (16). The different frequency offset images were registered to the unsaturated APT image using 2D rigid body registration with three degrees of freedom. The brain extraction tool (BET) in the FSL package (17) was used to remove the skull and non-brain tissue in the T_1 structural scan (including bias field correction). Since the field of view of the APT image in the z-direction was small, the brain of the unsaturated APT image was extracted by padding the end slices in both directions, copying the end slices several times, running the tool and then removing the added slices (option Z in BET). Subsequently the slice of the T_1 brain image which corresponded to the APT imaging plane was extracted and registered to the unsaturated APT brain using FLIRT.

The registered T_1 slice was then segmented using FMRIB's Automated Segmentation Tool (FAST) (18) into cerebrospinal fluid (CSF), grey and white matter (GM & WM) using a 0.1

Markov random field (MRF) beta value for main segmentation phase and bias field smoothing. The segmented brain regions were inspected after the automatic segmentation to remove regions of prior infarction, if any, by cross checking with the DWI data. The GM and WM marks were created using a 90% threshold on the partial volume estimates generated by FAST to obtain voxels that are as near as possible to pure GM or WM.

B_0 inhomogeneity was corrected using the shift in water centre frequency obtained by fitting the Bloch-McConnell equations (3 pools following (11)) to the collected CEST data (12,19). RMS differences between the average measured pre- and post-contrast z-spectra in the GM and WM, respectively, were calculated after the shift correction to estimate the associated percentage of change in T_1 in the post-contrast scans using the relationship derived from the simulations.

Magnetization transfer ratio (MTR) was calculated according to $MTR = 1 - M(\omega)/M_0$, where ω refers to saturation frequency offsets at ± 3.5 ppm and M_0 is the unsaturated signal. Only values of pre- and post-contrast MTR greater than 0 were included when studying the effect of Gd on MTR to filter out the noise in the measurement and unmasked non-brain area if any. MTR_{asym} , defined as $MTR(3.5\text{ppm}) - MTR(-3.5\text{ppm})$, was also calculated. Differences in the images of pre- and post-contrast were shown by subtraction (pre – post) after aligning them using FLIRT to minimize the movements between the scans.

Two-tailed unpaired t-tests were performed between the pre- and post-contrast MTR_{asym} in GM and WM respectively using the masks generated from FAST, to examine whether Gd had significant effect on the MTR_{asym} calculated. The statistical evaluations were done to the APT data in the GM and WM acquired both before and after the surgery in individual patients, and also at a group level, where the pre- and post-contrast data from all the patients in the GM or WM were grouped accordingly and then the t-tests were performed on them as a whole. In order to exclude the artefacts and noise near the boundary of the brain area, the t-tests were performed for the MTR_{asym} values from -0.05 to 0 (-5 to 0 %) only (the APT effect should be within this bound at 3T for the power used in this study (15,20)).

Results

Simulated and example measured z-spectra are shown in Figure 1, where the top left plot is the change of simulated z-spectra with different T_{1w} , and the remaining plots are measured post-surgery data: the first row shows the pre- and post-contrast average z-spectra in WM of representative patients 1 and 3, and their measured z-spectra in GM are shown in the bottom row. When the longitudinal relaxation of water pool T_{1w} was reduced in the simulation, the degree of saturation decreased, resulting in a z-spectrum with higher magnitude. In general, the change of measured z-spectra *in vivo* after Gd administration was consistent with the simulation. This change was observed for all the post-contrast z-spectra in GM and WM both before and after the surgery (Suppl. Figure 1 and 2).

Figure 2 (left) shows a linear relationship between the percentage of T_1 reductions (y) and RMS differences of the simulated pre- and post-contrast z-spectra formed using simulations, where $y = 576.4 * RMS + 0.05783$. The post-contrast T_1 reductions in the GM and WM of

each patient before and after surgery estimated using the relationship found are presented in Figure 2 (middle and right). The after surgery T_1 reductions were consistently higher in the GM and WM of all the patients when compared to the before surgery reductions. When assessing the T_1 change in the different compartment of the brain either before or after surgery, the percentage of reductions were always larger in the GM when compared to the WM. Before surgery, the post-contrast T_1 reductions were mostly below 10% across the brain for all the patients, except the change in GM of patient 4. After surgery, the reduction in the WM of all the patients was below 10% whereas the decrease was more than 10% but less than 20% in the GM.

Figure 3 shows the pre- and post-contrast, and pre- minus post-contrast difference in MTR and MTR_{asym} of all the patients both before and after the surgery. The red arrows in the figure indicate a prior infarct in patient 4 (cross-checked with DWI). In this region, both the MTR and MTR_{asym} had values similar to CSF in their respective measures.

Pre- and post-contrast MTR at ± 3.5 ppm in the segmented GM and WM of each patient before and after surgery are shown in Figure 4. The mean of post-contrast MTR values showed a decrease when compared to the pre-values, except before surgery MTR (-3.5ppm) in GM of patient 3. This was in good agreement with the observed z-spectra change in Figure 1.

The mean and standard deviation of MTR_{asym} in the GM and WM of each patient pre- and post-contrast are shown in Figure 5, along with the results of the t-tests. Significant differences between pre- and post-contrast MTR_{asym} at a 5% significant level were found in 25% of the patients recruited. Significance was also detected in WM at the group level both before and after surgery, but only in GM after surgery. Before surgery, GM of patient 4 and WM of patient 3 showed significant difference and after surgery, it was observed in GM and WM of patient 1. In the simulation, MTR_{asym} became less negative when T_{1w} reduced. The majority of the post-contrast values were less negative than the pre-contrast which is in agreement with the simulation but in a few cases (GM of patient 1 to 3 before surgery), the reverse was observed. Regardless of the presence or absence of Gd, the MTR_{asym} values were always more negative in the WM when compared to the GM.

Discussion

This study analysed the change of APT signal after the administration of Gd and performed statistical evaluations to examine whether the presence of residual Gd in the post-contrast APT imaging can cause quantification of the effect to be significantly different from its pre-contrast values. According to the simulations, when the longitudinal relaxation time of water protons decreases, the degree of saturation decreased, resulting in a z-spectrum with higher magnitude. In general, all the post-contrast z-spectra acquired *in vivo* both before and after the surgery were in agreement with the simulations. The change resulted in a pre- and post-contrast difference in the MTR images, with the majority of brain regions exhibited a positive difference.

Although APT imaging was performed some time after the Gd infusion, residual Gd would be present within the blood stream and thus appeared to affect the quantification of MTR_{asym} . A previous work (2) has shown that MTR is sensitive to the changes in T_{1w} induced by Gd; this has also been observed in our results. In theory, MTR_{asym} , defined as the difference of MTR at ± 3.5 ppm, should be less sensitive to this effect because it is an asymmetry measure, but the results in this study suggest that Gd may asymmetrically affect the APT spectrum, possibly related to the presence of NOE and/or dynamic spatial-temporal distribution of Gd in the brain during the post-contrast scan.

The MTR_{asym} values were found to be negative, contrary to the pure CEST saturation effect that would in theory result in a positive difference. This phenomenon has been widely observed and occurs due to a broad saturation effect at the negative frequency offsets of the z-spectrum attributed to NOE (20). A three pool model was used in the simulation with NOE and classical MT grouped as a single asymmetric pool in this study following (11,14). Although some studies modelled the effect using a fourth pool (21,22), it is still unclear how NOE might respond to Gd or be affected by the decrease of T_{1w} . This could modulate the MTR_{asym} , thus potentially explaining the variability in our results.

The differences of pre- and post-contrast z-spectra, and the estimated T_1 reductions were found to be larger in the GM when compared to the WM both before and after surgery. This is because GM is normally more perfused than WM, leading to higher quantity of Gd in the former and thus a larger influence on T_1 . When comparing the differences of pre- and post-contrast z-spectra, and estimated T_1 reductions before and after surgery, it was found that the differences and relaxation time reductions were greater after the surgery, most probably because the surgery would have increased the cerebral perfusion, leading to a higher residual of Gd in the post-contrast imaging.

In this study, data from 4 patients were analysed both before and after the surgery. Although the sample size was not big, significant differences in MTR_{asym} pre- and post-Gd administration were found in WM at the group level and in 25% of the patient results. Variability between individuals may arise due to the differences in perfusion as well as Gd clearance. The lower consistency of the results in the GM may be caused by the practical difficulty in segmenting the pure GM pixels. If the most conservative Bonferroni correction defined as α/n , where α is the significant level used - 5%, and n is the number of samples - 16, were applied to rule out significant differences in individuals within the group that arise by chance, p would need to be smaller than 0.0031. Using this more stringent p value for the statistical tests, there were still two cases where significance would be found at the individual level.

Consequently, the potential influence of Gd should be carefully considered when designing clinical protocols involving the contrast agents and APT imaging. This may be especially important for brain tumour imaging since there is a likelihood of Gd uptake in the cerebral tissue due to blood brain barrier breakdown and in acute ischemic stroke assessment since Gd will be lower in regions of low perfusion resulting from the blockage. Thus, if APT images are acquired after Gd infusion in these clinical scenarios, interpretation of the APT

effect using the widely used asymmetry measure would potentially be more complex, unless the T_{1w} change can be properly accounted for which is not the scope of this work.

Besides causing a reduction in T_{1w} , Gd also affects the transverse relaxation time of the water protons, T_{2w} , but its effect is less marked compared to the effect on T_{1w} (23). A decrease in T_{2w} broadens the linewidth of z-spectrum (24) and thus would affect the MTR_{asym} . However, the T_{2w} change is unlikely to substantially influence the results obtained in this study because there is minimal change on the linewidth of the measured z-spectra which suggests that the decrease of T_{2w} is negligible.

In this study, a single slice APT acquisition was used. Due to the patient movement between pre- and post-contrast APT scan and also differences in positioning before and after surgery, pixel-by-pixel comparison could not be performed to study the effect of residual Gd in the blood stream. Thus, the statistical evaluations had to be performed on the segmented GM and WM. It is likely that there will be spatial variations in the Gd effect on T_1 and thus MTR_{asym} due to local variations in perfusion as well as vascular topology.

Conclusions

This study suggests that MTR_{asym} values after the passage of Gd do not necessarily match those observed pre-contrast even though by being an asymmetry measure, it might be assumed to be insensitive to changes in T_1 . For quantitative APT imaging, this implies that it will be better to acquire APT data prior to the contrast agent administration to avoid potential misinterpretation of the APT effect, for inter-subject comparison or follow-up study.

Supplementary Material

Refer to Web version on PubMed Central for supplementary material.

Acknowledgements

YKT is funded by a Qualcomm Scholarship from Qualcomm Inc. MAC was employed by The Center of Excellence in Personalized Healthcare funded by the Wellcome Trust and EPSRC.

References

1. Sharma P, Socolow J, Patel S, Pettigrew RI, Oshinski JN. Effect of Gd-DTPA-BMA on blood and myocardial T 1 at 1.5T and 3T in humans. *J Magn Reson Imaging*. 2006; 23:323–330. [PubMed: 16456820]
2. Jones RA, Haraldseth O, Schjøtt J, et al. Effect of Gd-DTPA-BMA on magnetization transfer: application to rapid imaging of cardiac ischemia. *J Magn Reson Imaging*. 1993; 3:31–39. [PubMed: 8428099]
3. Zhou J, Payen J- Wilson DA, Traystman RJ, Van Zijl PCM. Using the amide proton signals of intracellular proteins and peptides to detect pH effects in MRI. *Nat Med*. 2003; 9:1085–1090. [PubMed: 12872167]
4. Sun PZ, Zhou J, Sun W, Huang J, Van Zijl PCM. Detection of the ischemic penumbra using pH-weighted MRI. *J Cereb Blood Flow Metab*. 2007; 27:1129–1136. [PubMed: 17133226]
5. Sun PZ, Wang E, Cheung JS. Imaging acute ischemic tissue acidosis with pH-sensitive endogenous amide proton transfer (APT) MRI-Correction of tissue relaxation and concomitant RF irradiation

- effects toward mapping quantitative cerebral tissue pH. *Neuroimage*. 2012; 60:1–6. [PubMed: 22178815]
6. Zhao X, Wen Z, Huang F, et al. Saturation power dependence of amide proton transfer image contrasts in human brain tumors and strokes at 3 T. *Magn Reson Med*. 2011; 66:1033–1041. [PubMed: 21394783]
 7. Zhou J, Tryggestad E, Wen Z, et al. Differentiation between glioma and radiation necrosis using molecular magnetic resonance imaging of endogenous proteins and peptides. *Nat Med*. 2010; 17:130–134. [PubMed: 21170048]
 8. Jia G, Abaza R, Williams JD, et al. Amide proton transfer MR imaging of prostate cancer: A preliminary study. *J Magn Reson Imaging*. 2011; 33:647–654. [PubMed: 21563248]
 9. Zhou J, Blakeley JO, Hua J, et al. Practical data acquisition method for human brain tumor amide proton transfer (APT) imaging. *Magn Reson Med*. 2008; 60:842–849. [PubMed: 18816868]
 10. Zhao X, Wen Z, Zhang G, et al. Three-Dimensional Turbo-Spin-Echo Amide Proton Transfer MR Imaging at 3-Tesla and Its Application to High-Grade Human Brain Tumors. *Mol Imaging Biol*. 2012:1–9.
 11. Chappell MA, Donahue MJ, Tee YK, et al. Quantitative Bayesian model-based analysis of amide proton transfer MRI. *Magn Reson Med*. 2012; 70:556–567. [PubMed: 23008121]
 12. Tee YK, Khrapitchev AA, Sibson NR, Payne SJ, Chappell MA. Evaluating the use of a continuous approximation for model-based quantification of pulsed chemical exchange saturation transfer (CEST). *Journal of Magnetic Resonance*. 2012; 222:88–95. [PubMed: 22858666]
 13. Deoni SCL. High-resolution T1 mapping of the brain at 3T with driven equilibrium single pulse observation of T1 with high-speed incorporation of RF field inhomogeneities (DESPOT1-HIFI). *Journal of Magnetic Resonance Imaging*. 2007; 26:1106–1111. [PubMed: 17896356]
 14. Hua J, Jones CK, Blakeley J, Smith SA, Van Zijl PCM, Zhou J. Quantitative description of the asymmetry in magnetization transfer effects around the water resonance in the human brain. *Magn Reson Med*. 2007; 58:786–793. [PubMed: 17899597]
 15. Jones CK, Polders D, Hua J, et al. In vivo three-dimensional whole-brain pulsed steady-state chemical exchange saturation transfer at 7 T. *Magn Reson Med*. 2012; 67:1579–1589. [PubMed: 22083645]
 16. Jenkinson M, Bannister P, Brady M, Smith S. Improved optimization for the robust and accurate linear registration and motion correction of brain images. *Neuroimage*. 2002; 17:825–841. [PubMed: 12377157]
 17. Smith SM. Fast robust automated brain extraction. *Hum Brain Mapp*. 2002; 17:143–155. [PubMed: 12391568]
 18. Zhang Y, Brady M, Smith S. Segmentation of brain MR images through a hidden Markov random field model and the expectation-maximization algorithm. *IEEE Trans Med Imaging*. 2001; 20:45–57. [PubMed: 11293691]
 19. Tee YK, Khrapitchev AA, Sibson NR, Payne SJ, Chappell MA. Optimal sampling schedule for chemical exchange saturation transfer. *Magn Reson Med*. 2013; doi: 10.1002/mrm.24567
 20. van Zijl PCM, Yadav NN. Chemical exchange saturation transfer (CEST): What is in a name and what isn't? *Magn Reson Med*. 2011; 65:927–948. [PubMed: 21337419]
 21. Jin T, Wang P, Zong X, Kim S. MR imaging of the amide-proton transfer effect and the pH-insensitive nuclear overhauser effect at 9.4 T. *Magn Reson Med*. 2012; doi: 10.1002/mrm.24315
 22. Liu D, Zhou J, Xue R, Zuo Z, An J, Wang DJJ. Quantitative characterization of nuclear Overhauser enhancement and amide proton transfer effects in the human brain at 7 tesla. *Magn Reson Med*. 2012; doi: 10.1002/mrm.24560
 23. Caravan P. Strategies for increasing the sensitivity of gadolinium based MRI contrast agents. *Chem Soc Rev*. 2006; 35:512–523. [PubMed: 16729145]
 24. Woessner DE, Zhang S, Merritt ME, Sherry AD. Numerical solution of the Bloch equations provides insights into the optimum design of PARACEST agents for MRI. *Magn Reson Med*. 2005; 53:790–799. [PubMed: 15799055]

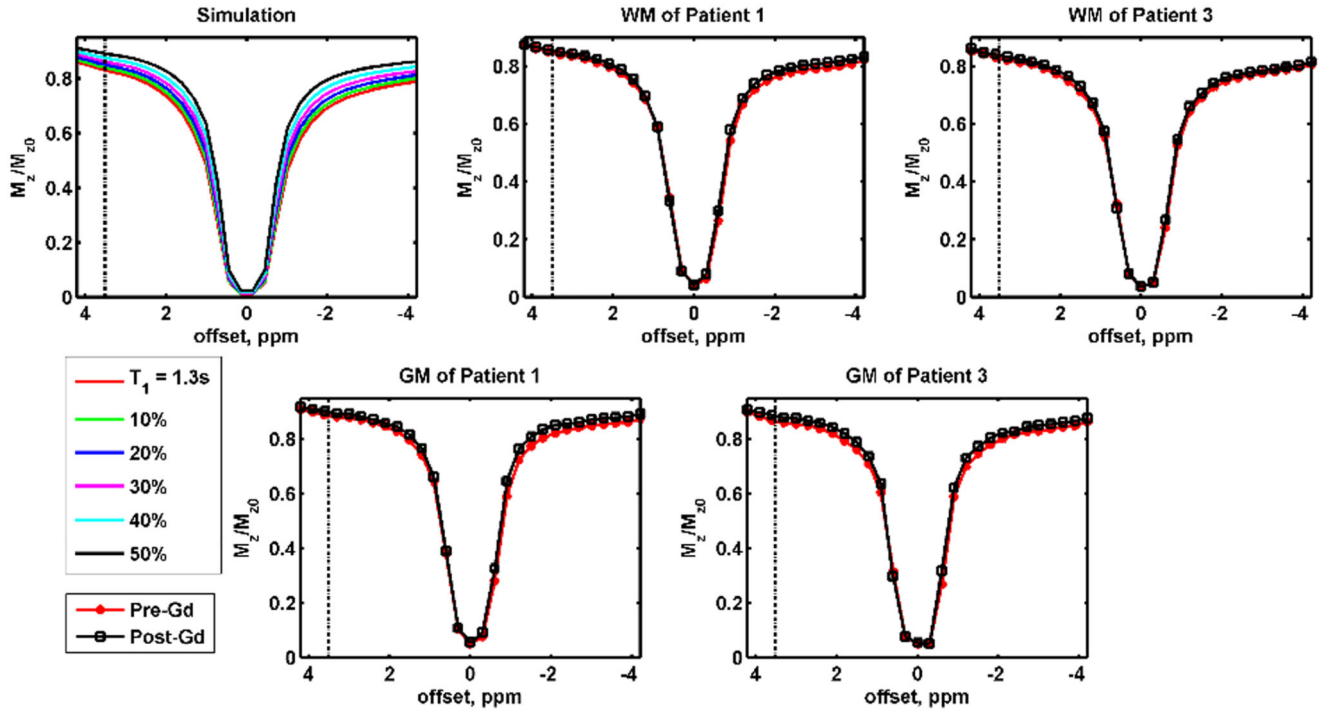


Figure 1.

The top left plot is the simulated z-spectra with different T_{1W} values, where $T_{1W} = 1.3$ s was used as the reference and the different colours represented T_{1W} was 10 to 50% less than the reference. The remaining plots in the first row are the experimentally measured z-spectra in WM of patient 1 and 3, and their z-spectra in GM are shown in the bottom row. All the measured results shown in this figure are the APT data collected after the surgery. The dot-dash lines are the chemical shift of amide protons (3.5 ppm).

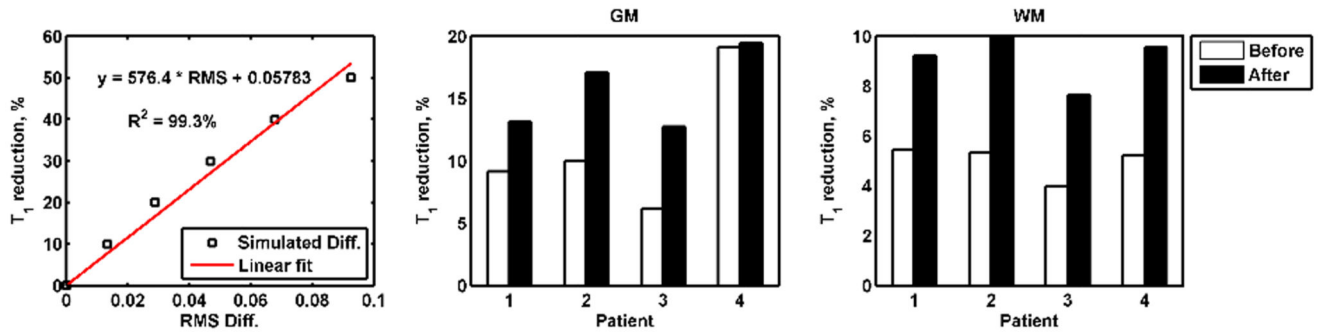


Figure 2. (left) A linear relationship between the percentage of T_1 change and RMS differences of the simulated pre- and post-contrast z-spectra was formed using simulation. Estimated post-contrast T_1 change in the GM (middle) and WM (right) of each patient before and after surgery based on the linear relationship found.

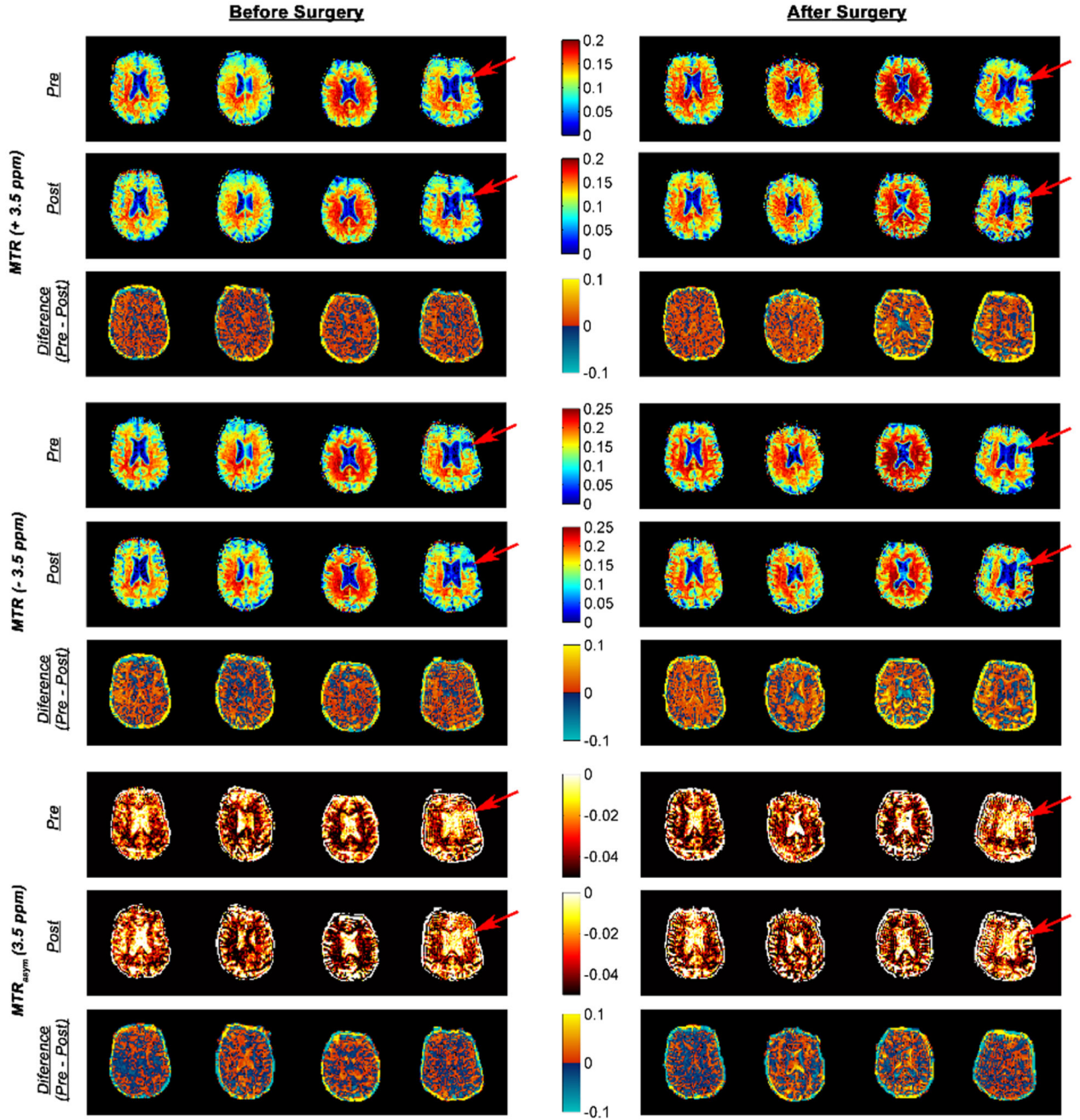


Figure 3.

Pre- and post-contrast MTR ($\pm 3.5 \text{ ppm}$) and $MTR_{\text{asym}} (3.5 \text{ ppm})$ of each patient before and after surgery. The difference of MTRs and MTR_{asym} pre- and post-Gd administration were plotted directly below their respective pre-images. The red arrows show a prior infarct in patient 4 (cross-checked with DWI data and found CSF-like signal in the area).

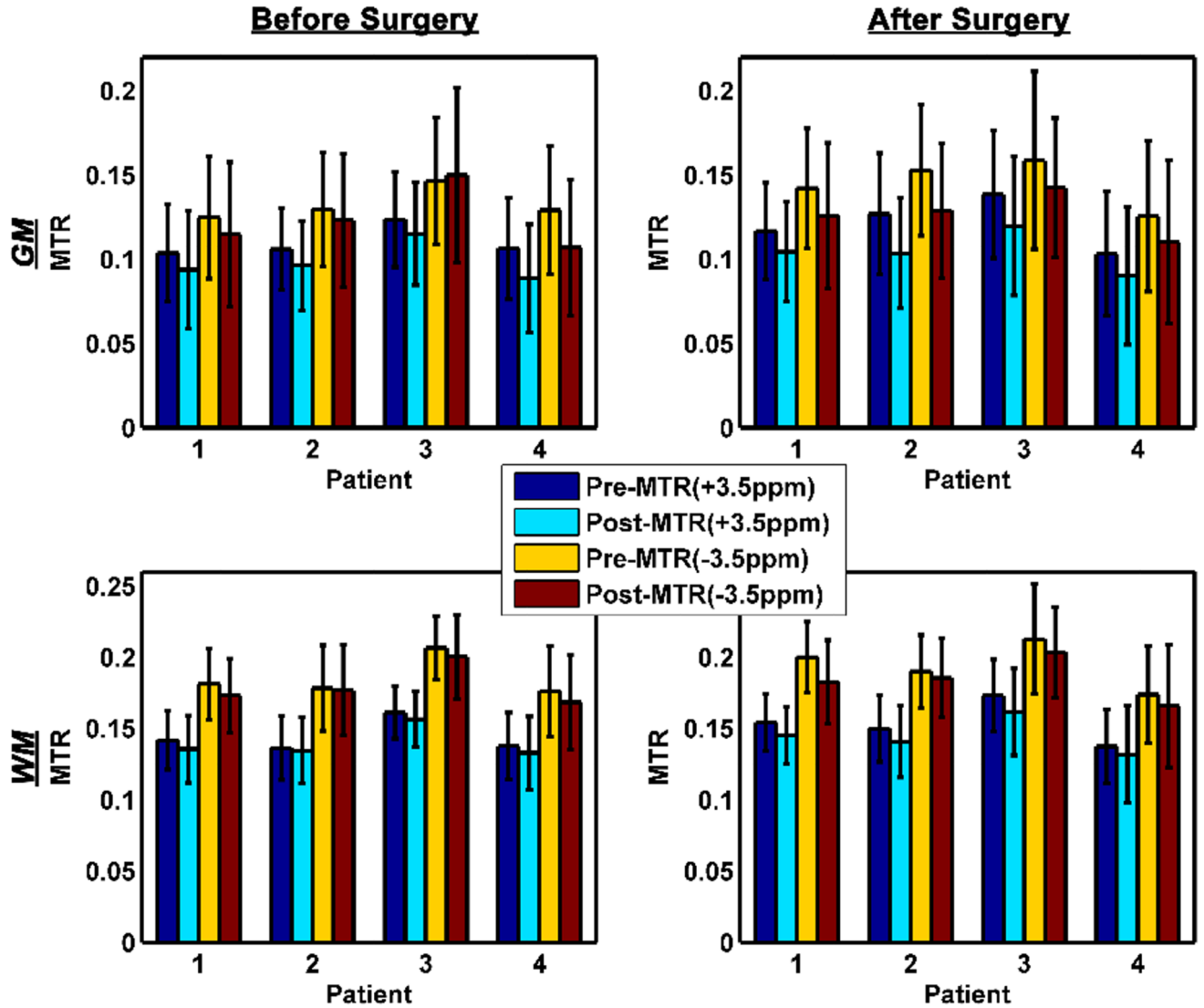


Figure 4.

Bar graphs with error bars showing the mean and standard deviation of pre- and post-contrast MTR values at ± 3.5 ppm, respectively, in the GM and WM of each patient. In order to minimize the noise in the measurement and imperfect segmentation, only MTR values greater than 0 were included.

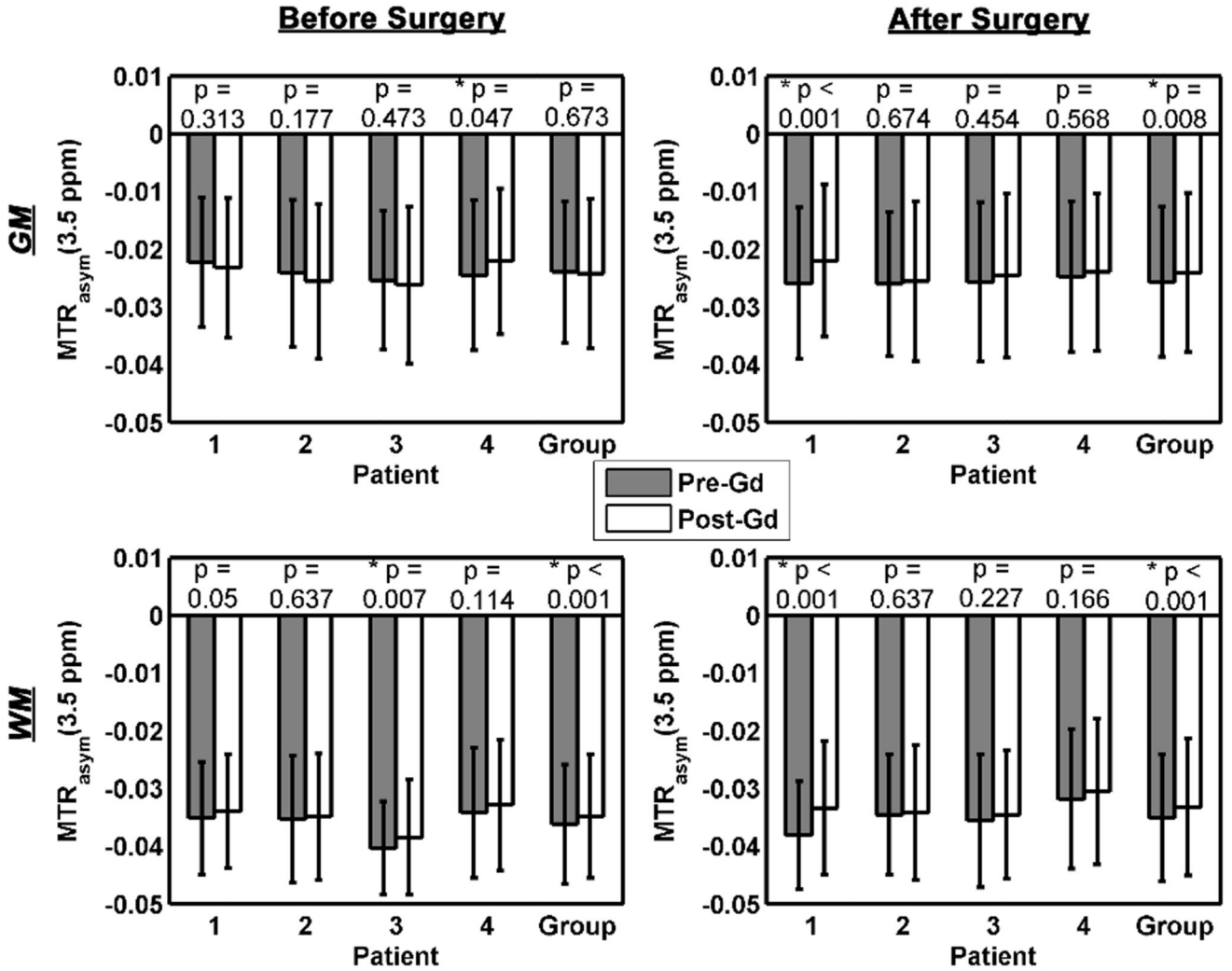


Figure 5. The bar graphs and error bars are the mean and standard deviation of MTR_{asyM} values, respectively, from -5 to 0 % before and after surgery in the GM and WM of each patient. Two-tailed unpaired t-tests were performed on the pre- and post-contrast MTR_{asyM} values in different region of the patient brain and also at the group level, where asterisks (*) refer to a significant difference found at a 5% significant level.